Lithos 117 (2010) 49–60

Contents lists available at ScienceDirect

Lithos

journal homepage: www.elsevier.com/locate/lithos

Metasomatic effects in the lithospheric mantle beneath the NE Bohemian Massif: A case study of Lutynia (SW Poland) peridotite xenoliths

Magdalena Matusiak-Małek [a,*], Jacek Puziewicz [a], Theodoros Ntaflos [b], Michel Grégoire [c], Hilary Downes [d]

[a] University of Wrocław, Institute of Geological Sciences, pl. M. Borna 9, 50-205 Wrocław, Poland
[b] University of Vienna, Department of Lithospheric Research, Althanstraße 14, 1090 Wien, Austria
[c] CNRS-UMR 5562, Univeristy of Toulouse, Observatoire Midi Pyrénées 14, av. E. Belin, 31-400 Toulouse, France
[d] Department of Earth and Planetary Sciences, Birkbeck University of London, Malet Street, London WC1E 7HX, UK

ARTICLE INFO

Article history:
Received 4 July 2009
Accepted 10 February 2010
Available online 19 February 2010

Keywords:
Lherzolite–harzburgite xenoliths
Upper mantle
Chromatographic metasomatism
SW Poland
Cenozoic basanite

ABSTRACT

Spinel lherzolite and spinel harzburgite mantle xenoliths occur in the 4.56 ± 0.2 Ma Lutynia basanite in SW Poland. Only one studied xenolith contains minor pargasitic amphibole. Minerals forming the xenoliths are chemically unzoned. Olivine (Fo $[(Mg/(Mg+Fe^{tot}))*100]_{89.8–92.4}$) contains 0.34–0.45 wt.% NiO and <780 ppm Ca; orthopyroxene is Al enstatite (#mg $[(Mg/(Mg+Fe^{tot})*100]$ 0.90–0.92, Al 0.06–0.17 a.pfu); clinopyroxene is Al–Cr diopside (#mg 0.91–0.93, Al 0.104–0.197 a.pfu). Exsolved orthopyroxene occurs in the clinopyroxene and vice versa. Al–Mg spinel occurs in symplectites with clinopyroxene. Second generation crystals of olivine ($Fo_{88.0–91.7}$, Ca up to 1800 ppm), clinopyroxene and spinel occur in small interstitial patches containing feldspar. Clinopyroxene II is Al-poor (0.018–0.070 a.pfu, #mg 0.921–0.932) when coexisting with alkali feldspar, but Al-rich (0.046–0.261 a.pfu; #mg 0.907–0.925) when found with plagioclase. Four types of REE (rare earth elements) patterns are found in the clinopyroxene: (group A) flat HREE (heavy REE) with LREE (light REE) content increasing smoothly; (group B) flat HREE with an abrupt increase of MREE (medium REE) and LREE; (group C) LREE-enriched, flat HREE with negative inflection at MREE; (group D) smoothly LREE-enriched with no flat HREE pattern. The exception is clinopyroxene from xenolith MM30 which is extremely depleted in LREE. Clinopyroxene I from all the xenoliths (excluding MM30) contains high amounts of Th and U.

Clinopyroxene trace element compositions record 8–15% of partial melting. Major and trace element compositions of minerals record later cryptic metasomatism induced by a CO_2-bearing alkaline melt. Variable REE patterns for clinopyroxene I from groups A, B and C are due to chromatographic enrichment, with group A peridotites located close to the metasomatic source and group C being the furthest. The pargasite-bearing MM04 was probably the closest to the metasomatic source and thus recorded incipient modal metasomatism.

Clinopyroxene–spinel symplectites and ortho-/clinopyroxene exsolutions suggest that the peridotites were transported from the garnet-lherzolite facies into the spinel one where they cooled and equilibrated at 960–1000 °C. The patches formed by the second generation of minerals are the effect of pre-eruption infiltration by the basanitic melt.

1. Introduction

Late Cretaceous to Pleistocene basaltic rocks are widespread in Europe (Lustrino and Wilson, 2007). Their origin is associated with collision between the African and Euroasian plates which led to development of a lithospheric rift system in the northern foreland of the Alps and uplift of Variscan basement blocks (Massif Central, Rhenish Massif, Bohemian Massif; Wilson and Downes, 2006).

Cenozoic lavas are common in the Bohemian Massif. The Eger Graben is the largest occurrence but numerous smaller ones are located in the NE part of the Massif (Sudetes and the Fore-Sudetic Block in SW Poland and N Czech Republic). More than three hundred outcrops of volcanic rocks, mostly basanites, nephelinites and basalts, are known from SW Poland (Ladenberger et al., 2006). They are concentrated in two large (Lubań–Frydlant and Złotoryja–Jawor) and three smaller (Niemcza–Strzelin, Niemodlin and Lądek Zdrój) volcanic fields in the Sudetes and in the Fore-Sudetic Block (Fig. 1a). Blusztajn and Hart (1989) and Ladenberger et al. (2006) showed that the lavas are derived from a heterogeneous mantle source including DMM, EM and HIMU components. Volcanic activity in SW Poland occurred in two main episodes: Late Oligocene (33.7–31.3 Ma) and Early Miocene (24.5–21 Ma; Birkenmajer et al., 2004). A third episode, the youngest, is

* Coresponding author. Tel.: +48 71 375 9296.
E-mail addresses: magdalena.matusiak@ing.uni.wroc.pl (M. Matusiak-Małek), jacek.puziewicz@ing.uni.wroc.pl (J. Puziewicz), theodoros.ntaflos@univie.ac.at (T. Ntaflos), michel.gregoire@dtp.obs-mip.fr (M. Grégoire), h.downes@ucl.ac.uk (H. Downes).

0024-4937/$ – see front matter © 2010 Elsevier B.V. All rights reserved.
doi:10.1016/j.lithos.2010.02.005

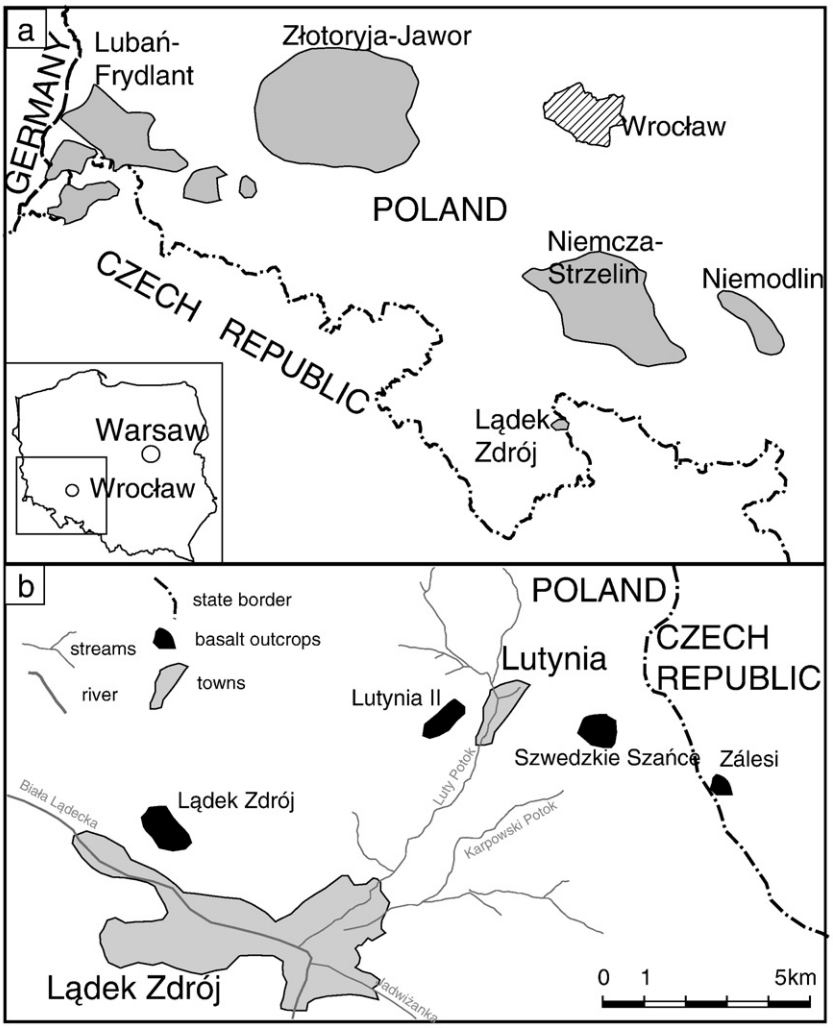

Fig. 1. (a) Cenozoic volcanic fields in SW Poland. Based on a map of Badura and Przybylski (2000); (b) basaltic rocks in the vicinity of Lądek Zdrój. Based on 1:100 000 geological map of Sawicki (1995).

recorded only in Lądek Zdrój (5.46 ± 0.2–3.83 ± 0.17 Ma; Birkenmajer et al., 2002). Young volcanic activity occurred also in the Czech (i.e. southern) part of the Sudetes (Bruntal area, 3.69 ± 0.56 Ma to 0.8 ± 0.11 Ma; Foltýnová, 2003; Kozákov volcano, 4–6 Ma; Šibrava and Havliček, 1980).

Mantle xenoliths occur in some of the lavas in SW Poland and were described from Lądek Zdrój (Blusztajn and Shimizu, 1994; Kozłowska-Koch, 1976), Złotoryja–Jawor vicinity (Białowolska, 1980) and Lubań (Bakun-Czubarow and Białowolska, 2003; Puziewicz, 2005). They are mostly anhydrous peridotites. Amphibole-bearing peridotites have been only described at Wołek Hill (Napieralska and Muszyński, 2006) and Wilcza Góra, where amphibole is associated with phologopite (Matusiak-Małek; unpublished data). In the present paper we describe mantle xenoliths in Cenozoic volcanic rocks from Lądek Zdrój area located in the Sudetes Mts.

2. Regional geology

Outcrops of Variscan basement can be followed through Western and Central Europe from Portugal and Spain through France and Germany and into to the Czech Republic and Poland. The eastern part of the Variscan orogen in Europe, i.e. the Bohemian Massif, is limited by the Sudetes Mts. in the north-east. Basanitic lavas, carrying mantle xenoliths described in this paper, occur in the Orlica–Śnieżnik dome (Western Sudetes Mts.). The dome consists of supracrustal formations (micaschists with intercalations of marble, quartzite and amphibolite) in synforms and orthogneisses in antiforms. Rocks forming the dome record medium to high grade metamorphism. Ultrahigh pressure (>2.7 GPa) conditions are recorded in eclogitic rocks in the eastern part of the dome (Bröcker and Klemd, 1996). The supracrustal series is assumed to be Neoproterozoic (Mazur et al., 2006). U–Pb and Pb–Pb zircon ages indicate that the magmatic protolith of the orthogneisses intruded 500 Ma ago (Oliver et al., 1993; Turniak et al., 2000; Kröner et al., 2001).

The Tertiary basanites of the Śnieżnik dome belong to the Central European Volcanic Province (CEVP). In this paper we describe mantle xenoliths from Lutynia village ("Szwedzkie Szańce" quarry; Fig. 1b) near Lądek Zdrój. They occur in a basanitic volcanic plug (Wierzchołowski, 1993) dated at 4.56 ± 0.2 Ma (K–Ar age; Birkenmajer et al., 2002). The basanite also carries clinopyroxene megacrysts and xenoliths of the crustal basement (gneisses, granites, quartzites; Kozłowska-Koch, 1976). Other xenolith occurrences in the Lądek Zdrój area comprise: Zalési (Czech Republic; Fediuk and Fediuková, 1985), Lutynia II and Lądek Zdrój (Kozłowska-Koch, 1976); all three outcrops are at present inactive quarries. The Lutynia (Szwedzkie Szańce and Lutynia II), Lądek Zdrój and Zalési are located 3–4 km from each other and probably form a single volcanic structure (Fig. 1a).

3. Analytical methods

Our study is based on major and trace element analyses of minerals in fourteen xenoliths. The modal compositions were established by an image analysis method (Higgins, 2000). The major element composition of minerals was obtained on >120 μm thick polished sections by using EMP Cameca SX-50 (Observatoire Midi Pyrénées, University Toulouse III) and Cameca SX-100 (University of Vienna, Department of Lithospheric Research). Operating conditions in both the used microprobes were identical. The accelerating voltage and beam current were 15 kV and 20 nA, respectively; PAP correction procedure was applied and natural and synthetic phases were used as standards. The counting times were extended to achieve detection limits of 200 ppm for Ca, 320 ppm for Cr and 400 ppm for Ni.

Concentrations of REE and other trace elements in clinopyroxene were determined in situ on a Cetac LSX-266 laser ablation module coupled with an Agilent 7500 ICP–MS instrument (Observatoire Midi Pyrénées, University Toulouse III). The NIST 610 and NIST 612 glass standards were used to calibrate relative element sensitivities. Each analysis was normalized using CaO values determined by electron microprobe. A beam diameter of 50–100 μm and a scanning rate of 20 μm/s were used. The theoretical detection limits range from 10–20 ppb for REE, Ba, Th, U, Zr to 2 ppm for Ti. The accuracy on a typical laser analysis is between 1 and 10%. The clinopyroxene trace element data set also includes new analyses of clinopyroxene separates from Lutynia investigated by Blusztajn and Shimizu (1994). They were mounted in epoxy resin and analyzed using a New Wave Research UP213 LASER coupled to an Agilent 7500a quadrupole ICP–MS system at the Research School of Earth Sciences Birkbeck/UCL. A laser diameter of 55 μm and a pulse frequency of 20 Hz were used, with a laser dwell time of 20 s.

Whole-rock analyses of the peridotites were not performed as the size of the xenoliths was too small to separate a sufficient amount of bulk rock without contaminations by host basanite-related veinlets.

The Morimoto (1989) classification scheme is used for pyroxenes, while for spinel we use Haggerty (1991) and Leake et al. (1997) for amphibole. Mineral abbreviations are: Ol (olivine), Cpx (clinopyroxene), Opx (orthopyroxene), Sp (spinel), Af/Pl/Fsp (alkali feldspar/plagioclase/feldspar), and Amp (amphibole). Fo stands for forsterite [(Mg/(Mg + Fe))*100], #mg for Mg/(Mg + Fe^{tot}), while #cr for Cr/(Cr + Al); cation ratios are given per formula unit (a.pfu). An (anorthite) content is (Ca/(Ca + K + Na))*100% and the Or (orthoclase) content is (K/(Ca + K + Na))*100%, which are the cation ratios per formula unit of feldspar. Spinel chemical composition was recalculated for three cations; Fe^{2+} and Fe^{3+} contents were calculated by charge balance according to Deer et al. (1993).

Temperatures were calculated using the Opx–Cpx geothermometers of Wells (1977) and Brey and Köhler (1990a) assuming a pressure of 1.5 GPa. Temperatures were calculated for at least 3 (mostly 5 or more) pairs of Opx/Cpx of the same generation.

4. Petrography of xenoliths

The mantle xenoliths are angular to oval and vary in size from 1 to 10 cm, but one sample (MM30) is an elongate 5 × 20 cm wide apple-green xenolith. Most have protogranular textures (Mercier and Nicolas, 1975) and only two grade into the porphyroclastic type (MM15, MM30; Fig. 2a, b). The grain size varies from 200 μm to >1 cm (see below). Kink bands occur in some olivine grains. Xenolith MM04 displays a weak foliation defined by elongation of Ol and Opx grains.

Most of the xenoliths are Sp harzburgites (7 samples) and Sp lherzolites (6 samples; Fig. 3; Table 1). One plots on the lherzolite/harzburgite boundary in the classification diagram. Subscripts I, II and III are used to indicate generation of a mineral: I = rock-forming minerals, II = second generation, minerals occurring in patches, and III = exsolution in generation I mineral.

Olivine I and Opx I form large crystals (200 μm–1.5 cm), while Ol II (15–50 μm) occur as small crystals within patches. Clinopyroxene I occurs as large (100–600 μm), isolated grains but also forms symplectites (up to 1 cm long) with Sp I (100 μm–1 cm) in most xenoliths (Fig. 2c). Patches (from 150 to 600 μm long) formed by subhedral to vermicular crystals of Cpx II (1–50 μm) ± Ol II (15–50 μm) ± rounded relicts of Opx I (1–50 μm) ± Sp II (single μm) ± Pl/Af occur between grains of Opx I ± Ol I ± Cpx I ± Sp I in all the xenoliths (Fig. 2d). In some xenoliths the patches occur not only at the grain boundaries but also inside Opx I crystals (Fig. 2e). Fringes of small (ca. 5 μm) brown crystals of Sp II embedded in an Af matrix often surround Sp I crystals in contact with these patches. Scarce vermicular grains of Cpx II, Ol II and Af or Pl occur at the margins of Opx I in some xenoliths (Fig. 2f).

Elongated exsolution lamellae (10–100 μm, in extreme cases up to 1 cm long) of Sp III occur in Opx I and Cpx I crystal cores. These Sp III lamellae are accompanied by Opx III lamellae in Cpx I and by Cpx III lamellae in Opx I grains. In scarce grains of Opx I, Cpx I and Ol I, rounded inclusions of Sp III (50–200 μm in diameter) occur. In xenolith MM04 the Opx III/Cpx III and Sp III lamellae are accompanied by 20 μm-long, oval exsolutions of amphibole. Rims of crystals which show exsolved cores are always clear (Fig. 2g).

Reaction zones between xenolith and host basanite occur in 5 of our samples. They are formed either by 20–100 μm in diameter/length rounded or elongated crystals of olivine or only slightly underlined by lighter (in BSE image) rims of minerals (mainly Opx I and Ol I) reacting with the basanitic melt (Fig. 2h). Some xenoliths contain veins of infiltrated host lava which can be traced from the contact with the surrounding basanite. These veins are up to 100 μm wide, and are filled with anhedral to subhedral crystals of feldspar as well as minute crystals of opaque oxides and apatite (Fig. 2h).

5. Mineral chemical and geochemical composition

5.1. Mineral major element composition

Forsterite content in Ol I varies from 89.8 to 92.4% (Fig. 4) and NiO content varies from 0.34 to 0.45 wt.% (Supplementary Table 1). The Ca content ranges from the microprobe detection limit (200 ppm) to 780 ppm. Marginal parts of Ol I grains in contact with patches are characterized by low NiO content (ca. 0.28 wt.%) and high Ca content (ca. 1000 ppm).

Olivine II within the patches is characterized by Fo and NiO contents slightly lower than those in Ol I ($Fo_{88.0}$ versus $Fo_{91.7}$ and 0.18 versus 0.42 wt.%, respectively; Supplementary Table 1). The Ca content is generally higher than in Ol I and reaches 1800 ppm.

Orthopyroxene I and Opx III have the same composition of Al enstatite or enstatite (in xenoliths MM25 and MM30; Fig. 5a–c). Their #mgs are 0.90–0.92, while the Al content varies from 0.06 to 0.17 a.pfu (Supplementary Table 2).

The composition of Cpx I (Ca 0.842–0.902 a.pfu) from all the xenoliths, except MM30, is Al–Cr diopside, (#mg 0.91–0.93, Al = 0.104–0.197 a.pfu, Cr = 0.016–0.34 a.pfu; Supplementary Tables 3 and 4, Fig. 5a). The Na content varies from 0.035 to 0.074, whereas the Ti content is negligible (<0.005 a.pfu). The relationships between #mg and Al and between Ca and Na, which allow good discrimination between the clinopyroxenes, are shown in Fig. 5d, e. Clinopyroxene I in xenolith MM30 is exceptional for its extremely high #mg (0.943–0.948) and Ca content (0.901–0.924 a.pfu) and low Al content (0.079–0.097 a.pfu; Supplementary Tables 3 and 4, Fig. 5a). Clinopyroxene II has a variable composition depending on the type of feldspar occurring in a given patch (Fig. 5b). Clinopyroxene II coexisting with Pl is Cr–Al (± Ti) augite or rarely Cr–Al–Ti diopside, whereas Cpx II associated with Af is mostly Cr augite, rarely Cr diopside (Fig. 5b, Supplementary Tables 3 and 4). Clinopyroxene III forming lamellae is a Al–Cr diopside/augite; the composition of Cpx III is similar to that of Cpx I from the same xenolith, except for lower

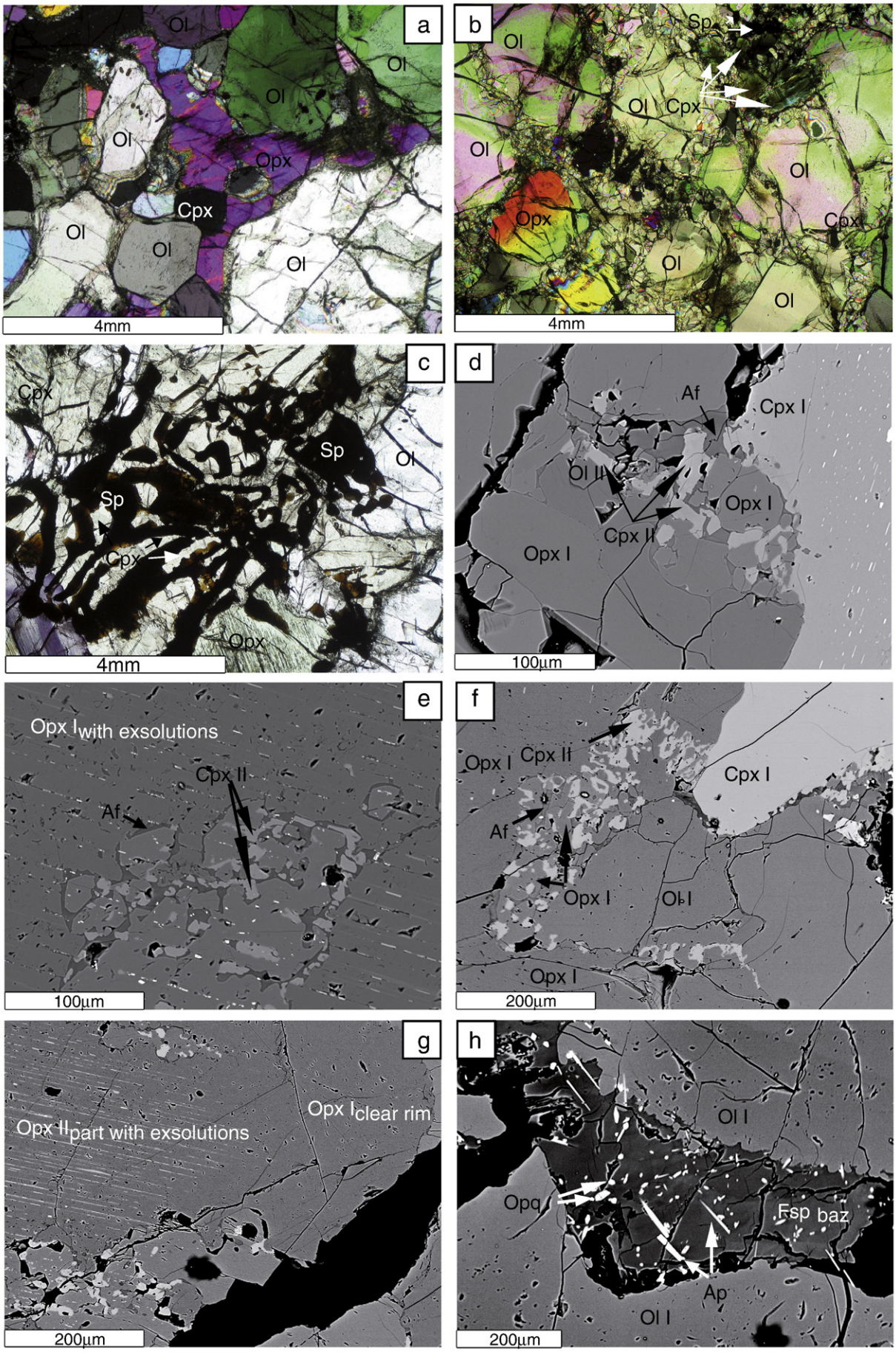
a
Ol
Ol
Ol
Ol
Opx
Cpx
Ol
Ol
Ol
4mm
b
Sp
Ol
Ol
Cpx
Ol
Opx
Ol
Cpx
Ol
Ol
4mm
c
Cpx
Sp
Ol
Sp
Cpx
Opx
4mm
d
Af
Cpx I
Ol II
Opx I
Cpx II
Opx I
100µm
e
Opx I with exsolutions
Cpx II
Af
100µm
f
Opx I
Cpx II
Cpx I
Af
Opx I
Ol I
Opx I
200µm
g
Opx I clear rim
Opx II part with exsolutions
200µm
h
Ol I
Opq
Fsp baz
Ap
Ol I
200µm

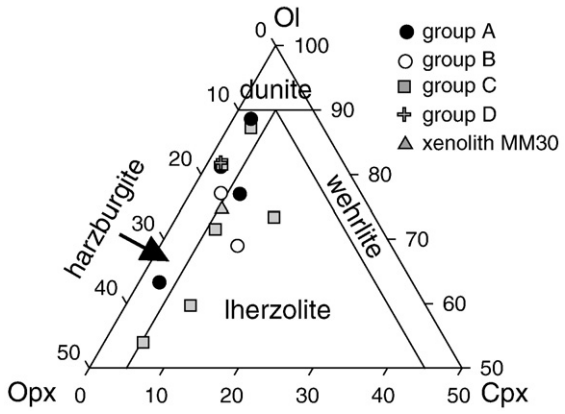

Fig. 3. Modal composition of xenoliths. The groups are defined based on the Cpx I REE composition, see Section "5.2 Clinopyroxene trace elements".

Table 1
Modal composition of xenoliths from Lutynia.

Xenolith	Ol [%]	Opx [%]	Cpx [%]	Sp [%]	Cpx trace element group
MM11	75.56	16.01	6.62	1.81	A
MM21	87.67	8.93	2.37	1.03	
MM22	62.34	33.44	2.73	1.49	
MM39	78.84	16.31	2.01	2.85	
MM03	51.60	38.91	5.00	4.48	B
MM08	71.97	13.26	12.87	1.90	
MM15	84.40	9.37	2.97	3.26	
MM29	57.64	30.44	8.39	3.53	
MM31	69.71	21.77	6.00	2.52	
MM09	68.05	20.37	10.27	1.32	C
MM25	75.29	18.37	4.03	2.30	
MM28	80.54	16.07	1.74	1.66	
MM04	80.27	16.12	2.02	1.59	D
MM30	72.96	19.44	5.35	2.25	MM30

#mg (Fig. 5d) and Ca content (Fig. 5e) as well as slightly higher Ti content (Supplementary Tables 3 and 4).

Spinel I is Al and Mg rich; its Cr content is commonly 0.330–0.523 a.pfu (#cr 0.168–0.271). However, in xenoliths MM04 and MM30 Cr is 0.612–0.669 a.pfu (#cr 0.314–0.347) and in MM15 it is 0.880–0.896 (#cr 0.459–0.472; Supplementary Table 5; Fig. 4). The #mg in Sp I varies from 0.722 to 0.837, only in xenolith MM15 it is 0.678–0.690. The Ti content is low, up to 0.015 a.pfu. Spinel II has variable chemical composition, i.e. Cr content 0.427–0.936 a.pfu (#cr 0.230–0.488), #mg 0.647–0.786. The Ti content in some Sp II grains is elevated to 0.020 a.pfu (Supplementary Table 5). Spinel III forming lamellae in Cpx I, Opx I and inclusions in Ol I has a variable Cr content from 0.300 to 0.521 a.pfu (#cr 0.157–0.269; Supplementary Table 5), only Sp III in MM04 and MM30 contains 0.307–0.619 a.pfu of Cr (#cr 0.161–0.337; Supplementary Table 5). The #mg of Sp III in all the xenoliths is similar (0.716–0.868) and the Ti content is low (<0.006 a.pfu).

The composition of Fsp from the patches is extremely variable, ranging from plagioclase to alkali feldspar (Supplementary Table 6). The anorthite content in Pl reaches 48%, while the Or content in Af reaches 52% (Supplementary Table 6, Fig. 6). Plagioclase (An 37–46; Ab 51–58) and Af (An 4–14, Ab 49–71, Or 14–45) also occur in veins of host lava crosscutting the xenoliths. They closely resemble those of their equivalents in the host basanite (Af An_{3-13}, Ab_{48-74}, Or_{13-48}; Pl An_{41-50}, An_{41-50}; Supplementary Table 7, Fig. 6).

Amphibole in xenolith MM04 is pargasite (Supplementary Table 7). Its #mg is 0.88–0.89, Na content is variable ranging from 0.84 to 0.93 a.pfu, while the Cr and K contents are rather constant (0.20–0.21 a.pfu and 0.15–0.16 a.pfu, respectively).

5.2. Clinopyroxene trace elements

Four main types of rare earth elements (REE) patterns, all characterized by light REE (LREE) enrichment and a flat pattern for heavy REE (HREE) but displaying slight differences, occur in Cpx I grains.

The first group (group A) is characterized by smooth "spoon-shaped" REE pattern ($La_N/Lu_N = 4.91–20.90$; $La_N/Sm_N = 2.76–4.21$) with flat HREE pattern ($Dy_N/Lu_N = 1.04–1.38$; Fig. 7a). The second group (group B) is LREE-enriched ($La_N/Lu_N = 8.50–55.29$, $La_N/Sm_N = 4.63–17.53$., Fig. 7c), with a strong increase in concentration from Eu (Dy in xenolith MM15) to La. The third group (group C) is characterized by steep La–Pr (Nd–Sm–Dy) negative inflection ($La_N/Lu_N = 3.06–11.92$; $La_N/Sm_N = 10.05–16.39$; Fig. 7e). The REE pattern of the group D shows a constant increase of LREE content ($La_N/Lu_N = 7.30–8.34$; Supplementary Table 8; Fig. 7a). The pattern becomes flat from Nd to La ($Nd_N/La_N = 0.88–1.12$).

Clinopyroxene I in xenoliths from all the groups contains relatively high amounts of Th and U and low amounts of Ba (Fig. 7a–f). Ta content is always low and varies between groups ($Ta_{N\ groupA} = 1.50–3.11$, $Ta_{N\ groupB} = 0.61–1.55$, $Ta_{N\ groupC} = 0.35–1.62$, $Ta_{N\ groupD,\ xen.\ MM04} = 5.86$). Xenoliths MM15 and MM29 which, according to their REE patterns, belong to group B have $Ta_N = 0.10$ and $Ta_N = 0.15$, respectively. Almost all the xenoliths display a negative Zr and Ti anomaly (group A: $La_N/Zr_N = 4.47–18.65$, $La_N/Ti_N = 15.65–67.52$; group B: $La_N/Zr_N = 82.10–182.44$ (302 and 203 in xenoliths MM15 and MM29, respectively), $La_N/Ti_N = 44.92–142.55$ (591.75 in xenolith MM15); group C: $La_N/Zr_N = 77.26–168.50$ $La_N/Ti_N = 10.16–51.16$; group D: $La_N/Zr_N = 1.20–1.57$, $La_N/Ti_{N\ xen.MM04} = 12473.11$). Clinopyroxene I is characterized by decreasing Zr/Hf ratio from group A to C (group A: 35.61–164.56, group B: 5.71–42.96, group C: 1.94–16.95) while in group D the ratio is very high (69.36–88.54), but lower than the highest values from group A. The REE content in Cpx I from xenolith MM30 differs from those of all the groups described above in that its REE abundances are all strongly depleted ($La_N/Lu_N = 0.07$ and $Lu_N = 0.37$, Fig. 7e–f). Its Hf content is below detection limit.

6. Temperature and pressure estimations

Temperatures obtained on clear rims of Opx I and Cpx I by different methods are in good agreement with each other, which suggests that the minerals were in chemical equilibrium (Supplementary Table 9). Equilibration temperatures of Cpx I and Opx I range from 960 °C to 1000 °C (Supplementary Table 9). Those calculated using Cpx III lamellae in Opx I and Opx III lamellae in Cpx I fall in the same range.

Since all the xenoliths are spinel facies peridotites, calculation of their pressure of equilibration is difficult due to the lack of reliable geobarometers. Spinel is stable between 0.9 (Presnall et al., 2002 and references therein) and 1.55 GPa (Klemme and O'Neill, 2000 and references therein) at 1000 °C. The spinel–pyroxene symplectites originated by garnet decomposition due to pressure decrease and cooling. We speculate that the uplift of garnet facies peridotites into the spinel facies is more likely over a short distance and thus the post-

Fig. 2. Phase relationships and texture of xenoliths from Lutynia. (a) Protogranular texture (xenolith MM09) sensu Mercier and Nicolas (1975) occurring in most xenoliths. Optical image, crossed polarizers; (b) porphyroclastic structure in xenolith MM15. Optical image, crossed polarizers; (c) vermicular crystals of Sp I and Cpx I forming a symplectite. Xenolith MM08, optical image, crossed polarizers; (d) "patch" filled with small crystals of Cpx II, Ol II and anhedral Af. Plagioclase may occur instead of Af. Xenolith MM29, BSE image; (e) "patch" filled with minerals as in (d) inside an exsolved core of Opx I. Xenolith MM31, BSE image; (i) crystals of Cpx II forming a vermicular rim around Opx I. Xenolith MM04, BSE image; (g) BSE image of Opx I crystals: the core contains lamellae of Cpx I II and Sp III, while the rim is exsolution-free. Xenolith MM08, BSE image; (h) feldspar and opaques (Opq) vein rooted in basanite intruding into the xenolith. Xenolith MM04, BSE image.

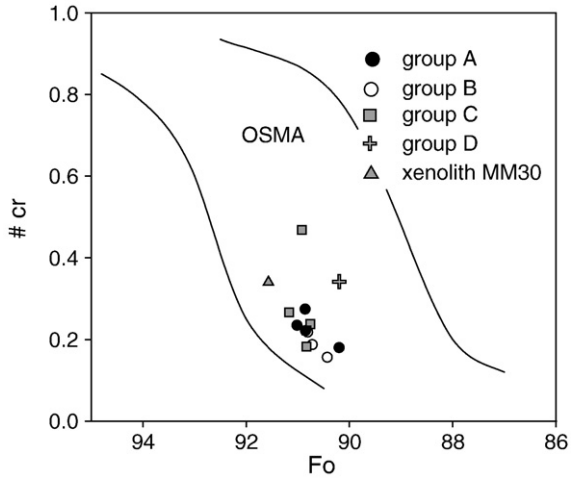

Fig. 4. Relationship between Fo content in Ol I and #cr in Sp I. All the xenoliths from Lutynia plot on the olivine–spinel mantle array (OSMA) of Arai (1994).

garnet symplectites originated close to the garnet-spinel boundary in the mantle, which was close to ca 1.55 GPa at 1000 °C.

7. Discussion

The history of mantle peridotites from Lutynia is recorded in the three generations of minerals. Orthopyroxene I and Cpx I grains contain abundant exsolutions lamellae of Cpx III, Opx III and Sp III. Clear rims and exsolved cores of host pyroxene grains have the same chemical composition (e.g. Fig. 5d–e) which indicates re-equilibration under spinel facies conditions and temperatures between 960 °C and 1000 °C. Pyroxene exsolutions indicate cooling of the peridotites as the miscibility gap between Cpx and Opx shrinks with decreasing temperature.

Clinopyroxene–spinel symplectites, like those from Lutynia, are often attributed to decomposition of garnet during re-equilibration of garnet peridotites in the Sp-stability field (e.g. Downes et al., 2003; Falus et al., 2007). The low degree of MREE(medium REE)/HREE fractionation in Cpx I that form symplectites ($(Sm/Yb)_N = 0.29–3.17$, except in xenolith MM15: 5.76) indicates that it was formed at the expense of garnet in the Sp-stability field; indeed if Cpx I has crystallized in equilibrium with garnet, the HREE would be preferentially incorporated in garnet resulting in $(Sm/Yb)_N > 5$ (Bonadiman et al., 2008 and references therein).

Decomposition of garnet may be due to heating or decompression. The studied peridotites are chemically well equilibrated and pyroxene exsolution suggests equilibration after cooling. Therefore, we conclude that the garnet decomposition was related to decompression and possibly cooling.

7.1. Partial melting

Variation in mineral composition in the Lutynia peridotites suggests that they are residues after melt extraction. This process is expressed by the variable and high #mg and low Al content in

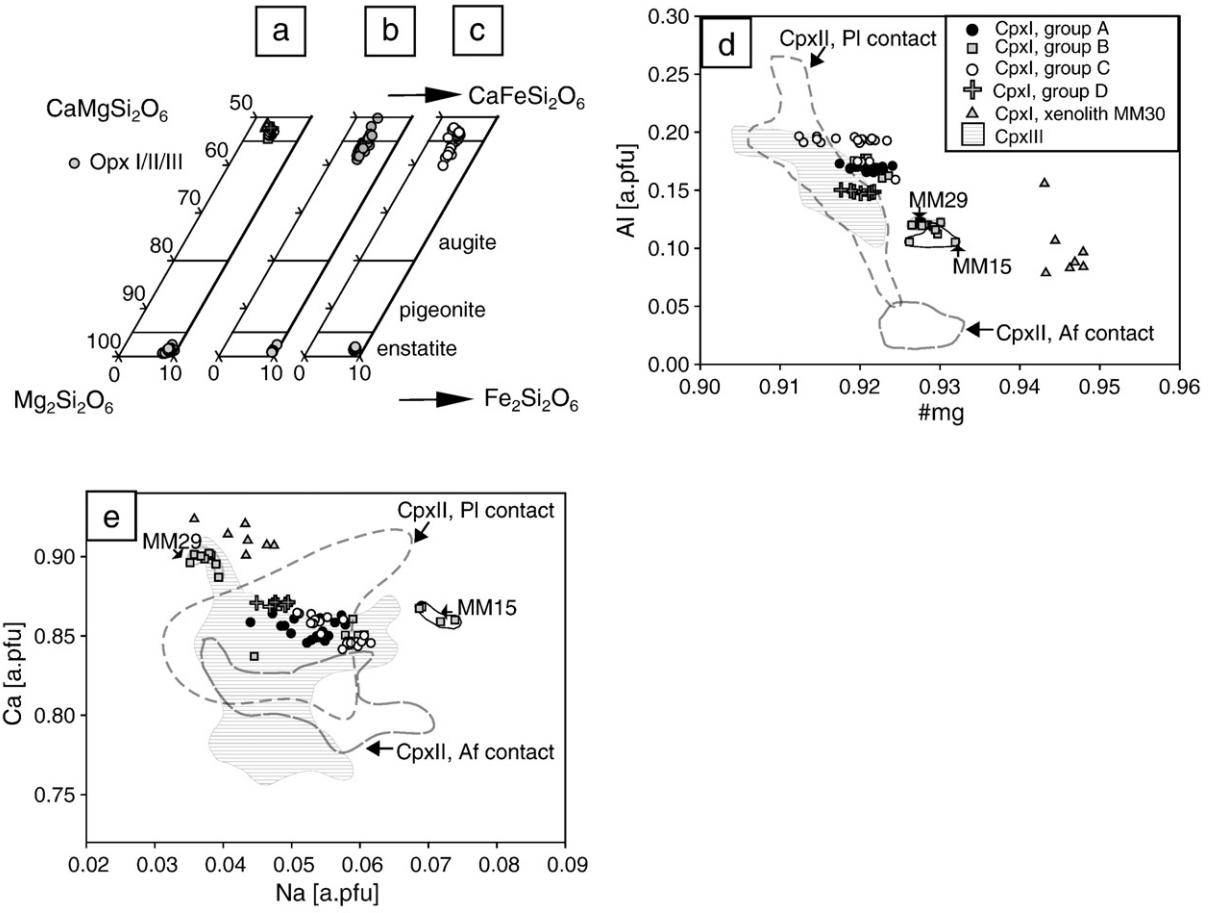

Fig. 5. Major element composition of Cpx and Opx. (a) Points representing Cpx I and Opx I on the Fs–Wo–En classification diagram. (b) Points representing Cpx II and Opx II on the Fs–Wo–En classification diagram. (c) Points representing Cpx III and Opx III on the Fs–Wo–En classification diagram. (d) Relationships between #mg and Al contents in Cpx I, Cpx II and Cpx III. (e) Relationships between Ca and Na contents in Cpx I, Cpx II and Cpx III; field symbols as in (d).

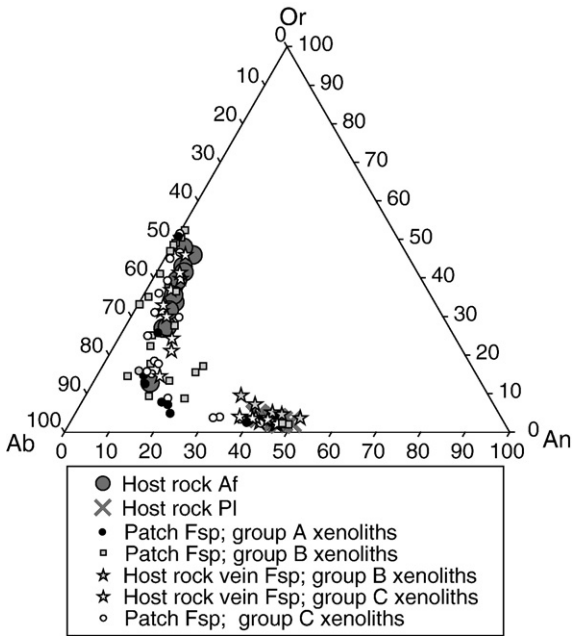

Fig. 6. Points representing Fsp from patches and host basanite in the An–Or–Ab diagram.

pyroxenes, high Fo content in Ol I, the negative correlations of #mg vs. Al and Ti vs. Yb contents in Cpx I, and the negative #mg vs. #cr correlation in Sp I. Negative correlations between #cr and Yb and Lu also suggest that distribution of these elements in Cpx I was controlled by partial melting rather than by metasomatism (Ackerman et al., 2007).

As rare Amp grains occur in only one of the xenoliths and no phlogopite is present, Cpx I is the main host for REE. The partial melting degree may therefore be estimated based on the assumption that Cpx I controls the distribution coefficient for Lu and Yb in the residuum (Norman, 1998). We have calculated the amount of extracted melt using both batch and fractional melting models. For the starting bulk composition of the mantle (C_0) and fraction of diopside in the source (X_{Cpx}), we have assumed the same values as Norman (1998; see Fig. 8). The modeling suggests that batch melting would require an unrealistically high degree of partial melting (Norman, 1998), whereas Yb_N/Lu_N ratios in Cpx I fit the fractional melting model very well, giving results ranging between 7 and 15% (Fig. 8). However, the calculated partial melting degree in xenolith MM30 is about 27%. This result is problematic as so high degree of melt extraction would remove clinopyroxene I entirely from the rock. Thus we assume, that this result is an artifact and new Cpx may have crystallized in the rock because of metasomatism (see Section 7.3).

7.2. Metasomatism

Trace element composition of Cpx I (e.g. elevated REE content, Sr/Ce ratios lower and La/(La/Yb) ratios higher than in undepleted primitive mantle) reveals that the Lutynia peridotites were metasomatically enriched. Most of the xenoliths from Lutynia have been affected by cryptic metasomatism which is recorded only in the trace element composition of Cpx I.

Blusztajn and Shimizu (1994) suggested (on the base of Ti/Zr ratio and U-shaped clinopyroxene REE patterns) that peridotites from Lutynia have been enriched by a carbonatitic melt. Carbonatite metasomatism is supported by the strong LREE-enrichment and high Th and U contents (e.g. Touron et al., 2008 and references therein) and moderate to strong negative anomalies in Ti and Zr in groups B and C. High Zr/Hf ratios also suggests a carbonatitic affinity of the metasomatic agent (Dupuy et al., 1992). In the $(Ti/Eu)/(Yb/Lu)_N$ diagram by Coltorti et al. (1999), Cpx I from Lutynia group A and B xenoliths plot in carbonatite field. On the other hand, the trace element composition of Cpx I does not display the other basic features assigned to carbonatite metasomatism, i.e. positive Sr anomaly and Ta–Ba contents above the primitive mantle level (e.g. Coltorti et al., 1999; Ionov et al., 2002). Moreover, Dantas et al. (2009) suggested that high Th and U contents as well as negative Ti anomalies may be an effect of "random percolation of (alkaline to sub-alkaline) melt within the mantle column". Thus, a typical carbonatite metasomatic agent is not conclusively supported for the Lutynia mantle peridotites.

The incompatible trace element compositions of Cpx I from Lutynia are similar to those from the Ray Pic mantle xenoliths (French Massif Central; Zangana et al., 1997; 1999). Xenoliths from both occurrences (i.e. groups A, B and C from Lutynia and LREE-enriched protogranular, protogranular/porphyroclastic and porphyroclastic peridotites from Ray Pic) display similar REE patterns characterized by strong Th, U and LREE-enrichment. Zangana et al. (1997; 1999) proposed an alkaline fluid/melt as the metasomatic agent for peridotites from Ray Pic. By analogy, an alkaline fluid/melt is a possible metasomatic agent for Lutynia xenoliths.

To test this hypothesis we have calculated a melt in equilibrium with the clinopyroxene of group D xenoliths. We have used only this clinopyroxene, as its REE pattern displays a continuous enrichment in REE, which is a typical pattern for Cpx in equilibrium with an alkaline melt. It also does not record any significant melting processes. The REE patterns of other samples (groups A, B and C and xenolith MM30) show strong evidence for both melting (HREE) and enrichment (LREE) processes, thus they cannot be totally in equilibrium with any melt. We assume that the significant differences in REE patterns between groups result from their different distance from the source of the metasomatic agent (chromatographic effect as proposed below).

For computing the composition of a fluid in equilibrium with group D xenoliths, we have used Cpx/alkali basalt partition coefficients dataset given in Table 2. The theoretical melt in equilibrium with group D xenoliths is strongly LREE- and MREE-enriched, while HREE are flat (Fig. 9). Such a REE pattern is typical for an alkaline silicate melt. The carbonatite imprint recorded in Cpx I trace element composition (i.e. Ti and Zr anomalies, high Th/U contents, high Zr/Hf ratios), may result from different amounts of volatiles, most probably CO_2, present in the alkaline silicate melt (as discussed by Ionov et al., 2002, Grégoire et al., 2009).

The REE patterns of Cpx I in groups A, B and C are similar to those of Cpx of mantle xenoliths from Spitsbergen (Ionov et al., 2002), Oman (Grégoire et al., 2009) and Cameroon (Teitchou, personal communication). These authors propose a two-stage evolution model to explain the geochemical features of mantle samples they investigated. First, an upper mantle domain experienced partial melting, which caused depletion in incompatible elements—especially LREE. Later, a metasomatic melt of alkaline affinity, more or less CO_2-enriched, circulated within the previously depleted mantle resulting in its enrichment in incompatible elements. A similar two-stage model may be applied to the Lutynia mantle xenoliths investigated in our study.

Trace element composition of group D xenoliths, despite REE patterns differing significantly from the patterns of other groups, is in general similar to the trace element composition of groups A, B and C (Fig. 7b, d, f). Thus, we assume that all the investigated mantle xenoliths were metasomatised by a similar alkaline and probably CO_2-bearing agent. According to the chromatographic metasomatism model of Ionov et al. (2002), the depleted mantle which is located closest to the magmatic source (vein, dyke) of the metasomatic agent is percolated by a relatively large volume of melt which enriches it all of the incompatible trace elements including the whole suite of REE. This may explain also the crystallization of purely metasomatic phases such as amphibole. Such a strongly enriched mantle is represented in

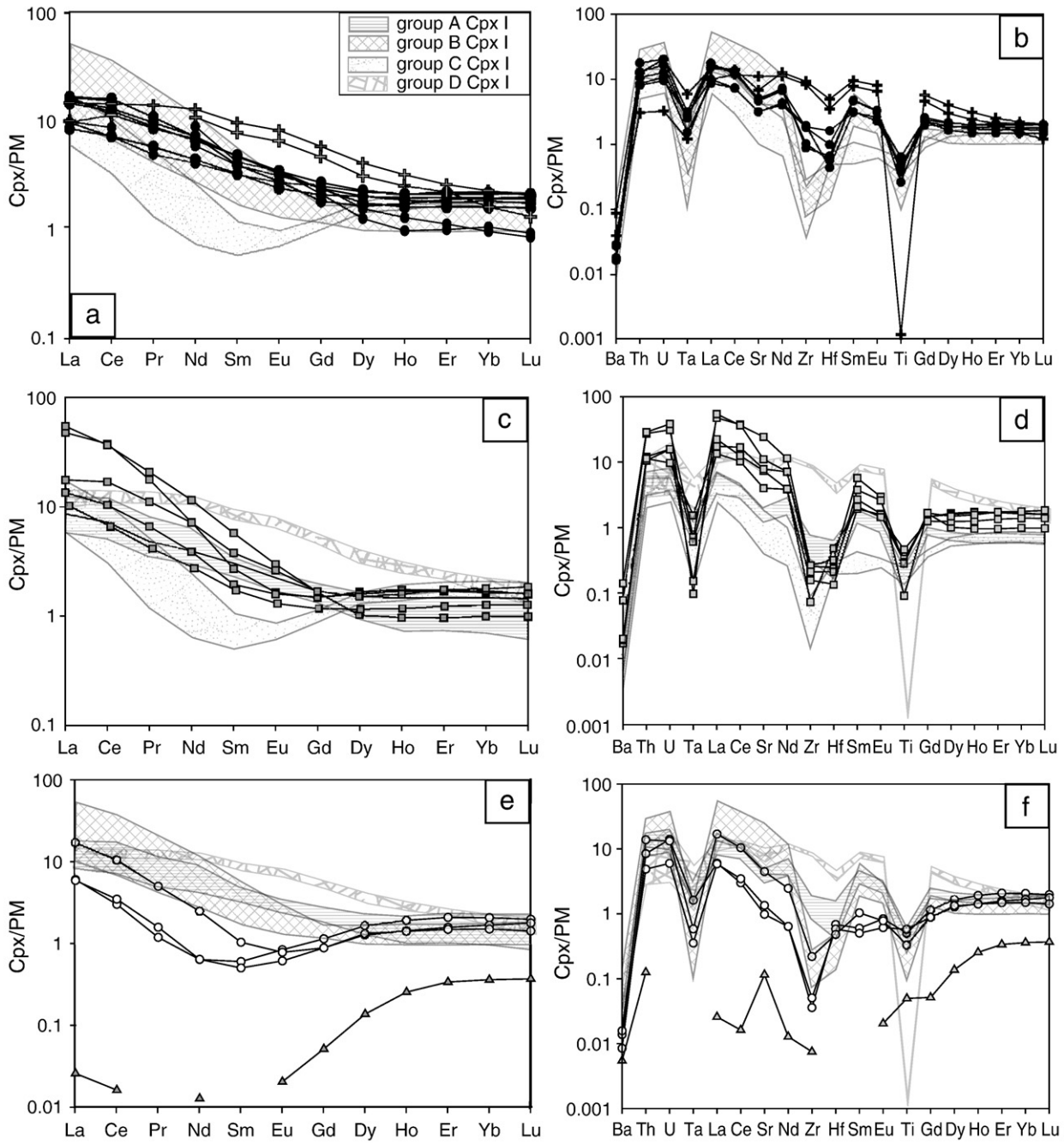

Fig. 7. Trace element composition of Cpx I. (a) Primitive mantle-normalized (McDonough and Sun, 1995) REE patterns for groups A and D Cpx I. (b) Primitive mantle-normalized incompatible element patterns for groups A and D Cpx I. (c) Primitive mantle-normalized REE patterns for group B Cpx I. (d) Primitive mantle-normalized incompatible element patterns for group B Cpx I. (e) Primitive mantle-normalized REE patterns for group C and xenolith MM30 Cpx I.(f) Primitive mantle-normalized incompatible element patterns for group C and xenolith MM30 Cpx I.

the present study by group D xenoliths (Fig. 7a). As the metasomatising agent percolates through the mantle further from the source, its REE composition is continuously fractionated from the less incompatible (HREE) to the most incompatible (LREE) ones. Finally this mechanism of metasomatism superimposed on LREE-depleted patterns inherited from partial melting, may explain the variable shapes of REE patterns observed in metasomatised mantle peridotites from Lutynia: those relatively close to the "metasomatic source" are enriched either in the less incompatible and the most incompatible REEs (group A xenoliths), while in those located furthest from the source, only the most incompatible REE (LREE and MREE) are enriched (group B and C xenoliths, Fig. 7c–e).

7.3. Origin of variation in clinopyroxene chemical composition

Clinopyroxenes I from groups A, B (except for MM15 and MM29; see below) and C, display homogeneous chemical compositions within a given group. The relationship between major element composition and REE patterns of Cpx I suggests that its major element composition might have been affected by cryptic metasomatism. Alternatively, the slightly higher Na/Ca ratio in group C clinopyroxenes (Fig. 5e) suggests that this group might have equilibrated at slightly higher pressures than group A and B xenoliths (Köhler and Brey, 1990).

Clinopyroxenes I and III from xenolith MM15 are highly magnesian (#mg = 0.93) and define a well separated group, enriched in Na

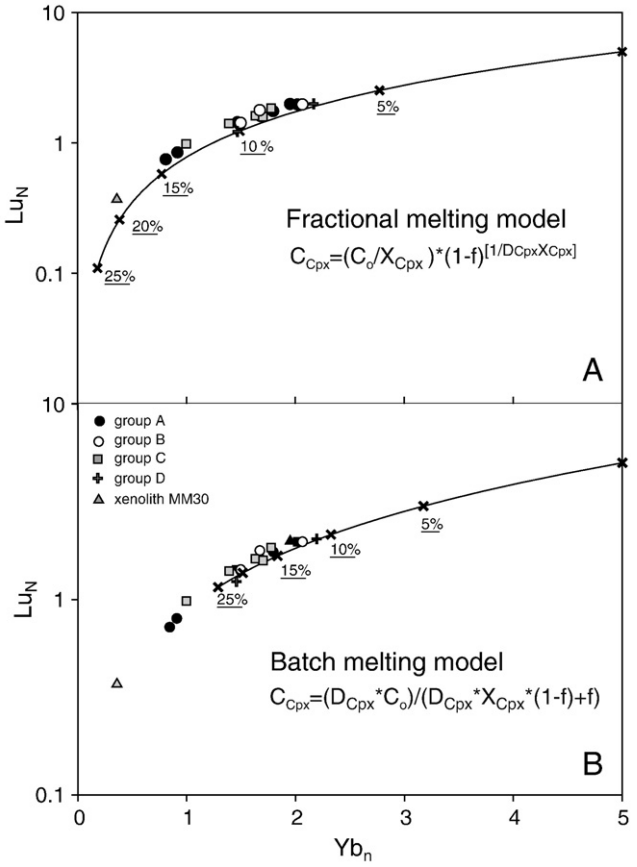

Fig. 8. Batch and fractional melting models based on Yb and Lu contents in Cpx I (Norman, 1998) compared with data from the Cpx I from xenolith from Lutynia. (A) Fractional melting model; (B) batch melting model. Formulae for the two models are given. Abbreviation and values used in the formulas: C_{Cpx}—concentration of trace element in diopside; C_0—starting bulk composition in the source (see text); X_{Cpx}—fraction of diopside in the source (see text); D_{Cpx}—crystal/liquid distribution coefficient: 0.40 for Yb and 0.35 for Lu; f—degree of partial melting. Symbol "N" stands for "normalized to primitive mantle values" (McDonough and Sun, 1995).

(>0.07 a.pfu) and of slightly lower Ca content. This xenolith displays porphyroclastic texture which, according to Mercier and Nicolas (1975), results from deformation of primary protogranular rock. The major element chemical composition of Cpx I in this xenolith may be a result of adaptation to conditions in which the deformation took place. Location of the deformation event in the mantle column is problematic, as clino- and orthopyroxene in xenolith MM15 are not in equilibrium and thus determination of their equilibration temperature is impossible and the temperatures calculated for the clino- and orthopyroxene exsolutions give contradictory results (Supplementary Table 9). The Sm_N/Yb_N ratio in Cpx I is 5.76 which suggest that this sample may represent a deeper part of the mantle, where Cpx I would be in equilibrium with garnet. Textures in almost all of the investigated xenoliths record its provenance from the garnet-stability field (clinopyroxene–spinel symplectites), but only in MM15 is the origin frozen into the trace element composition of Cpx I. On the other hand, the REE pattern as well as extended trace element diagram for Cpx I from this xenolith mimics the main trends characteristic for group B xenoliths; thus we assume that it was also enriched by CO_2-bearing alkaline melt suggested above.

The major element composition of Cpx I from xenolith MM29 exhibits a depleted nature (# mg = 0.93, Al = 0.12 a.pfu, Ca = 0.90 a.pfu, Na = 0.04 a.pfu; Fig. 5). However, the REE pattern classifies the xenolith as LREE-enriched B group (Fig. 7c). This xenolith may represent rocks furthest from the source of metasomatism, which preserved the chemical composition of pre-metasomatic clinopyroxene, and where only the trace element characteristic has been changed.

Table 2
The experimental Cpx-alkali basalt partition coefficients.
Data after Norman (1998).

Element	$D_{Cpx/melt}$
La	0.055
Ce	0.075
Nd	0.150
Sm	0.250
Eu	0.300
Gd	0.040
Dy	0.450
Ho	0.450
Er	0.450
Yb	0.400
Lu	0.350

The major and trace element compositions of minerals in xenolith MM30 make this sample exceptional due to their extremely depleted nature (Figs. 5d–e, 7e–f, and 8). The Al contents in Opx I and Cpx I differ significantly from bordering grains (e.g. 0.008 vs. 0.01 a.pfu) but do not differ between the two groups (0.06–0.10 and 0.08–0.10 a.pfu, respectively). Thus we suggest that Opx I and Cpx I in xenolith MM30 are not in equilibrium and that Cpx represents a crystallized melt. This xenolith may constitute a part of strongly depleted mantle which was further affected by a metasomatic melt. The intruding agent was depleted (Cpx I records an extremely high degree of partial melting) and carried only selected elements such as Sr, Ti and Th (Fig. 7e, f).

7.4. Late enrichment processes

Patches occurring between grains of rock-forming minerals are known in many mantle xenoliths worldwide; however their origin is still unclear (Shaw, 1999). The most striking feature of minerals occurring in such patches, mostly Ol II and Cpx II, is the change in their Ca contents in respect to Ol I (780 ppm in Ol I, 1800 in Ol II) and Cpx I (0.84–0.92 a.pfu in Cpx I, 0.69–0.91 in Cpx II). Feldspar occurring in patches is texturally later than Cpx II, Ol II and Sp II (e.g. Fig. 2d), thus the crystallization of second generation of minerals was followed by feldspar crystallization. Feldspar compositions vary continuously from Pl to Af. The alkali feldspar and plagioclase occurring in the host basanite fall within the range defined by feldspar from patches (Fig. 6). Thus we suggest that the patches are a manifestation of an infiltration of a melt whose chemical composition was similar to that of the host basanite. Infiltration must have taken place before the

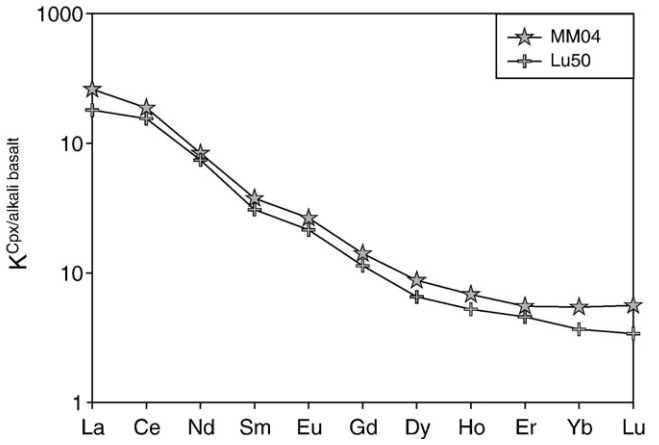

Fig. 9. Primitive mantle-normalized (McDonough and Sun, 1995) REE pattern for liquid in equilibrium with Cpx I from group D xenoliths. The REE content for liquid in equilibrium with MM04 and Lu50 was computed with partition coefficients given in Table 2.

eruption since the melt had time to react with primary minerals, resulting in crystallization of the second generation of minerals (i.e. Ol II, Cpx II, and Sp II). The composition of Cpx II and Sp II can originate under mantle conditions. The continuous chemical variation of feldspar in patches suggests that it crystallized at supersolvus conditions, thus at depths where high temperatures persisted during crystallization.

7.5. The upper mantle beneath the north-eastern part of the Bohemian Massif

Lutynia is one of the easternmost Cenozoic volcanic occurrences in the CEVP. Its xenoliths offer an opportunity to get information about the lithospheric mantle beneath the NE part of the Bohemian Massif at a relatively recent time (ca. 5 Ma). Xenolith-bearing Cenozoic lava occurrences of similar age also occur at Kozákov in the Sudetes (Ackerman et al. 2007), located ca 150 km WNW from Lutynia, and ca. 50 km from the Eger Graben in western part of the Bohemian Massif.

Christensen et al. (2001) compared data from xenolith fabrics and geothermometry with SKS shear wave splitting and *Pn* anisotropy and proposed a three layer model for the mantle beneath Kozákov. According to this, the upper (32–43 km) and lower (<67 km) layers are formed of equigranular peridotites, whereas the middle layer (43–67 km) is formed of protogranular peridotites. Formation of the layers was probably linked to Variscan convergence of the mantle.

The majority of the Lutynia xenoliths display protogranular textures, and the Cpx I major element composition (Fig. 10), estimated fractional melting degree, and Cpx trace element contents are similar to those of some xenoliths from Kozákov. The less-depleted equigranular peridotites from Kozákov (those subjected to 4.2–9% partial melting) and groups A and B from Lutynia display similar REE shapes in Cpx, despite some differences in absolute content of trace elements, especially HREEs (Fig. 11a). The same is true for patterns of the Kozákov protogranular (6.7–13.2% of partial melting) and group C xenoliths (Fig. 11b). Xenoliths containing clinopyroxene displaying REE characteristics similar to those of the upper layer of equigranular mantle from Kozákov were not found in Lutynia.

Clinopyroxenes in peridotites from Lutynia and Kozákov have similar major and trace element compositions (Fig. 10). However, the ranges of temperatures (Brey and Köhler, 1990) recorded in peridotites from both occurrences differ significantly: the lower equigranular and protogranular xenoliths from Kozákov record temperatures from 875 to 1116 °C while in the Lutynia xenoliths the temperatures vary in the narrow range 960–1000 °C. Clinopyroxene composition in both occurrences is similar, but the equilibration temperatures vary significantly. This results from different compositions of Opx especially Ca contents, which strongly affect the equilibration temperatures. Thus the Kozákov peridotites are petrographically different from those from Lutynia. However, the lava occurrence in Kozákov is much larger than that in Lutynia, and the discrepancies may result from different scales of mantle sampling.

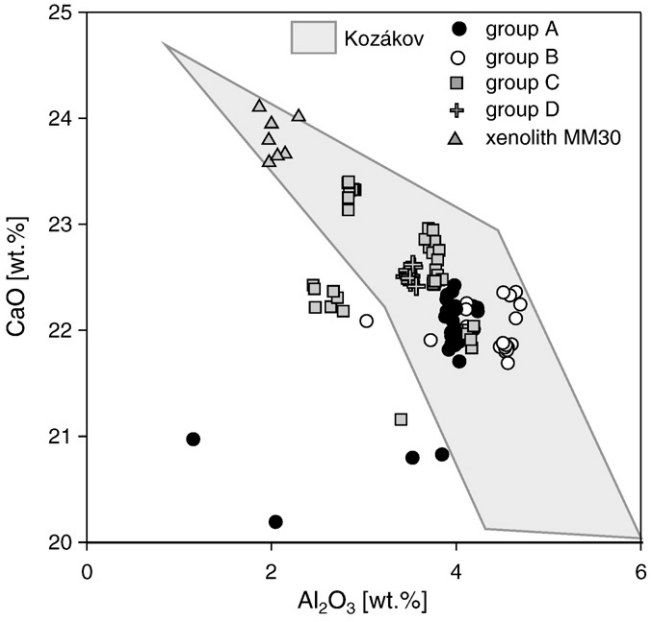

Fig. 10. Al_2O_3/CaO ratio in Cpx I from Lutynia compared to composition of Cpx from xenoliths from Kozákov (Czech Republic; Ackerman et al., 2007).

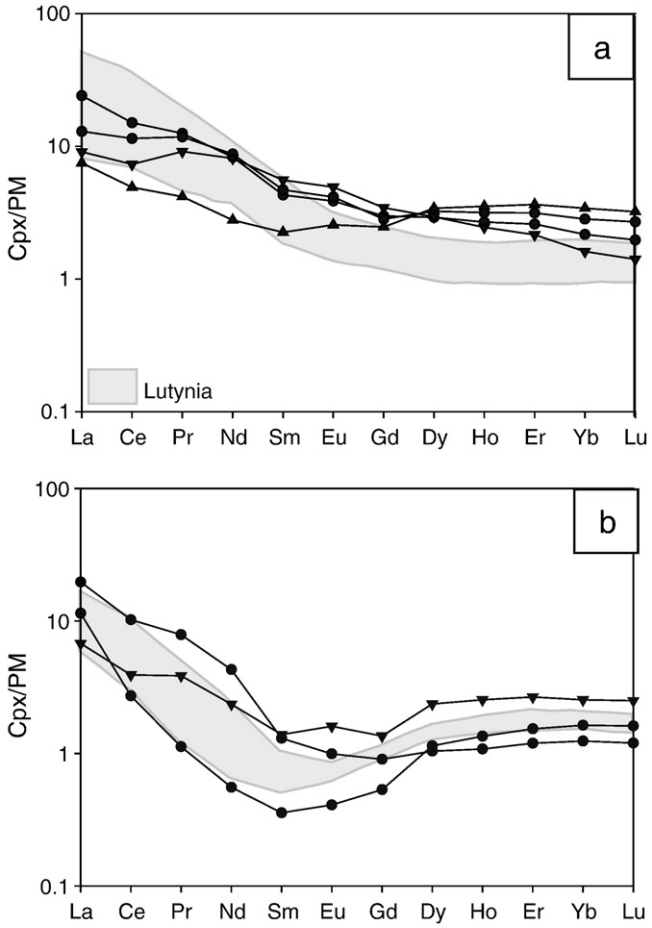

Fig. 11. Primitive mantle-normalized (McDonough and Sun, 1995) REE patterns in Cpx from Lutynia and Kozákov (Ackerman et al., 2007) (a) REE patterns of Lutynia groups A and B Cpx (grey field) and Kozákov lower equigranular xenoliths; (b) REE patterns of Lutynia group C Cpx (grey field) and Kozákov protogranular xenoliths.

8. Conclusions

The peridotite xenoliths at Lutynia represent the lithospheric mantle beneath the NE part of the Bohemian Massif at ca. 5 My. They equilibrated in a narrow temperature range of 960–1000 °C. Spinel–clinopyroxene symplectites and unmixing of ortho- and clinopyroxene suggest that their protoliths were garnet peridotites, that converted to spinel peridotites as temperatures and pressures decreased.

The Lutynia mantle underwent partial melting with melt extraction degrees mostly from 8 to 15%. The depleted peridotitic mantle was afterwards metasomatically refertilized. The peridotite supposedly closest to the metasomatic source contains minor amounts of pargasitic amphibole and its clinopyroxene REE content displays continuous enrichment from HREE to LREE. However, the metasomatism was almost entirely cryptic and is recorded only in the clinopyroxene

trace elements. The REE contents in the clinopyroxenes vary among the xenoliths forming three main REE patterns, differing in LREE and MREE content. We suggest that the different REE patterns are related to chromatographic enrichment by the same metasomatic agent. A carbonatitic metasomatism in Lutynia was proposed by Blusztajn and Shimizu (1994). Our study indicates that some features are in agreement with a carbonatitic imprint in peridotites from Lutynia, nevertheless their trace element contents suggest that a CO_2-bearing alkaline silicate melt is the most likely metasomatic agent.

Acknowledgements

We thank B.G.J. Upton and an anonymous reviewer for their constructive reviews which helped us to improve the manuscript. This paper is a part of the PhD study of the first author, the costs of which were covered from the project MNiSW N N307 100634 to JP. The microprobe data were acquired at the University of Vienna thanks to the Fellowship of Austrian Government to MMM, and the trace element data at the University of Toulouse thanks to the Fellowship of French Government to MMM. Some of the data was acquired thanks to the joint 2008–2009 project of the Department of Lithospheric Research, University of Vienna, and Institute of Geological Sciences, University of Wrocław, in the frame of Austrian–Polish scientific and cultural cooperation agreement. We are grateful to J. Blusztajn for providing mineral separates and to Caja de Vries for analyzing them.

Appendix A. Supplementary data

Supplementary data associated with this article can be found, in the online version, at doi:10.1016/j.lithos.2010.02.005.

References

Ackerman, L., Mahlen, N., Jellnek, E., Medaris Jr., G., Ulrych, J., Strnad, L., Mihaljevič, M., 2007. Geochemistry and evolution of subcontinental lithospheric mantle in Central Europe: evidence from peridotite xenoliths of the Kozákov volcano, Czech Republic. Journal of Petrology 48, 2235–2260.

Arai, S., 1994. Characterization of spinel peridotites by olivine–spinel compositional relationship: review and interpretation. Chemical Geology 113, 191–204.

Badura, J., Przybylski, B., 2000. Neotectonic Map of Lower Silesia. Central Geological Archive, Polish Geological Institute.

Bakun-Czubarow, N., Białowolska, A., 2003. Gabbroic enclaves from basaltoids of the Lubań and Złotoryja regions, Lower Silesia. Xth Meeting of the Petrology Group of the Mineralogical Society of Poland. Mineralogical Society of Poland, Głuchołazy, pp. 32–34.

Białowolska, A., 1980. Geochemiczna charakterystyka niektórych bazaltoidów Dolnego Śląska i ich ultramafitowych enklaw. Archiwum Mineralogiczne 36, 107–170 (in Polish).

Birkenmajer, K., Lorenc, M. W., Pécskay, Z., Zagożdżon, P.P., 2004. Wiek, cykle i kierunek migracji trzeciorzędowego bazaltowego wulkanizmu Dolnego Śląska w świetle datowań K–Ar. In: K.J.-Ś. M. Michalik, Skiba, M., Michalik,J., (Ed.), VIII Ogólnopolska Konferencja Naukowa "Datowanie minerałów i skał". Wydział Geologii, Geofizyki i Ochrony Środowiska AGH, Instytut Nauk Geologicznych UJ, Komitet Badań Czwartorzędu PAN, Kraków (in Polish).

Birkenmajer, K., Pécskay, Z., Grabowski, J., Lorenc, M.W., Zagożdżon, P.P., 2002. Radiometric dating of the Tertiary volcanics in Lower Silesia, Poland. II. K–Ar and paleomagnetic data from Neogene basanites near Lądek Zdrój, Sudetes Mountains. Annales Societatis Geologorum Poloniae 72, 119–121.

Blusztajn, J., Hart, R.S., 1989. Sr, Nd and Pb isotopic character of Tertiary basalts from southwest Poland. Geochimica et Cosmochimica Acta 53, 2689–2696.

Blusztajn, J., Shimizu, N., 1994. The trace-element variations in clinopyroxenes from spinel peridotite xenoliths from southwest Poland. Chemical Geology 111, 227–243.

Bonadiman, C., Coltorti, M., Duggen, S., Paludetti, L., Siena, F., Thirwall, M.F., Upton, B.J., 2008. Palaeozoic subduction-related and kimberlite or carbonatite metasomatism in the Scottish lithospheric mantle. Geological Society, London, Special Publication 293, 303–333.

Brey, G.P., Köhler, T., 1990. Geothermobarometry in four-phase lherzolites II. New thermobarometers and practical assessment of existing thermobarometers. Journal of Petrology 31, 1353–1378.

Bröcker, M., Klemd, R., 1996. Ultrahigh-pressure metamorphism in the Śnieżnik Mountains (Sudetes, Poland): P–T constraints and geological implications. Journal of Geology 104, 417–433.

Christensen, N.I., Medaris, L.G., Wang, H.F., Jelinek, E., 2001. Depth variation of seismic anisotropy and petrology in central European lithosphere: a tectonothermal synthesis from spinel lherzolite. Journal of Geophysical Research-Solid Earth 106 (B1), 645–664.

Coltorti, M., Bonadiman, C., Hinton, R.W., Siena, F., Upton, B.G.J., 1999. Carbonatite metasomatism of the oceanic upper mantle: evidence from clinopyroxenes and glasses in ultramafic xenoliths of Grande Comore, Indian Ocean. Journal of Petrology 40, 133–165.

Dantas, C., Grégoire, M., Koester, E., Conceição, R.V., Rieck, J.N., 2009. The lherzolite–websterite xenolith suite from Northern Patagonia (Argentina): evidence of mantle-melt reaction processes. Lithos 107, 107–120.

Deer, W.A., Howie, R.A., Zussman, J., 1993. An Introduction to the Rock-Forming Minerals. Longman Scientific & Technical, New York.

Downes, H., Reichow, M.K., Mason, P.R.D., Beard, A.D., Thirlwall, M.F., 2003. Mantle domains in the lithosphere beneath the French Massif Central: trace element and isotopic evidence from mantle clinopyroxenes. Chemical Geology 200, 71–87.

Dupuy, C., Liotard, J.M., Dostal, J., 1992. Zr/Hf fractionation in intraplate basaltic rocks: carbonate metasoamtism in the mantle source. Geochimica et Cosmochimica Acta 56, 2417–2423.

Falus, G., Szabó, C., Kovács, I., Zajacz, Z., Halter, W., 2007. Symplectite in spinel lherzolite xenoliths from the Little Hungarian Plain, Western Hungary: a key for understanding the complex history of the upper mantle of the Pannonian Basin. Lithos 94, 230–247.

Fediuk, F., Fediuková, E., 1985. Postmezozoické alkalické vulkanity severni Moravy. Acta Universitatis Carolinae – Geologica, Neužil 4, 355–382 (in Czech).

Foltýnová, R., 2003. Geochemicko – petrografická charakteristika neovulkanitů severni Moravy a Slezska. Masaryk University, Brno (in Czech), Master thesis.

Grégoire, M., Langlade, J.A., Delpech, G., Dantas, C., Ceuleneer, G., 2009. Nature and evolution of the lithospheric mantle beneath the passive margin of East Oman: evidence from mantle xenoliths sampled by Cenozoic alkaline lavas. Lithos 112, 203–216.

Haggerty, S.E., 1991. Oxide mineralogy of the upper mantle. In: Lindsley, D.H. (Ed.), Oxide Minerals: Petrologic and Magnetic Significance. Mineralogical Society of America, pp. 355–416.

Higgins, M.D., 2000. Measurement of crystal size distributions. American Mineralogist 85, 1105–1116.

Ionov, D.A., Bodinier, J.L., Mukasa, S.B., Zanetti, A., 2002. Mechanisms and sources of mantle metasomatism: major and trace element compositions of peridotite xenoliths from Spitsbergen in the context of numerical modeling. Journal of Petrology 43, 2219–2259.

Klemme, S., O'Neill, H. StC, 2000. The near-solidus transition from garnet lherzolite to spinel lherzolite. Contributions to Mineralogy and Petrology 138, 237–248.

Kozłowska-Koch, M., 1976. Petrography of ultramafic nodules in basaltoids from the environs of Lądek (Sudetes). Bulletin de l'academie Polonaise des Sciences 24, 67–76.

Köhler, T.P., Brey, G.P., 1990. Calcium exchange between olivine and clinopyroxene calibrated as a geothermobarometer for natural peridotites from 2 to 60 kb with applications. Geochimica et Cosmochimica Acta 54, 2375–2388.

Kröner, A., Jaeckel, P., Hegner, E., Opletal, M., 2001. Single zircon ages and whole-rock Nd isotopic systematic of early Paleozoic granitoid gneisses from the Czech and Polish Sudetes (Jizerske hory, Karkonosze Mountains and Orlica-Śnieżnik Complex). International Journal of Earth Sciences 90, 304–324.

Ladenberger, A., Michalik, M., Tomek, C., Peate, D.W., 2006. Alkaline magmatism in SW Poland — an example of astenosphere–litosphere interactions? Mineralogia Polonica Special Papers 29, 40–47.

Leake, B.E., Woolley, A.R., Arps, C.E.S., Birch, W.D., Gilbert, M.C., Grice, J.D., Hawthorne, F.C., Kato, A., Kisch, H.J., Krivovichev, V.G., Linthout, K., Laird, J., Mandarino, J.A., Maresch, W.V., Nickel, E.H., Rock, N.M.S., Schumacher, J.C., Smith, D.C., Stephenson, N.C.N., Ungaretti, L., Whittaker, E.J.W., Guo, Y.Z., 1997. Nomenclature of amphiboles: report of the subcommittee on amphiboles of the International Mineralogical Association, commission on new minerals and mineral names. American Mineralogist 82, 1019–1037.

Lustrino, M., Wilson, M., 2007. The circum-Mediterranean anorogenic Cenozoic igneous province. Earth-Science Reviews 81, 1–65.

Mazur, S., Aleksandrowski, P., Kryza, R., Oberc-Dziedzic, T., 2006. The Variscan Orogen in Poland. Geological Quarterly 50, 89–118.

McDonough, W.F., Sun, S.S., 1995. The composition of the Earth. Chemical Geology 120, 223–253.

Mercier, J.C.C., Nicolas, A., 1975. Textures and fabrics of upper-mantle peridotites as illustrated by xenoliths from basalts. Journal of Petrology 16 (2), 454–487.

Morimoto, N., 1989. Nomenclature of pyroxenes. Subcomission of new minerals and mineral names. International mineralogical association. Canadian Mineralogist 27, 143–156.

Napieralska, M., Muszyński, A., 2006. Peridotite enclaves in picrobasalts from Wołek Hill near Nowy Kościół (SW Poland) — preliminary data. Mineralogia Polonica Special Papers 29, 63–65.

Norman, M.D., 1998. Melting and metasomatism in the continental lithosphere: laser ablation ICPMS analysis of minerals in spinel lherzolites from eastern Australia. Contributions to Mineralogy and Petrology 130, 240–255.

Oliver, G.J.H., Corfu, F., Krogh, T.E., 1993. U–Pb ages from SW Poland: evidence for a Cadomian suture zone between Baltica and Gondwana. Journal of Geological Society 150, 355–369.

Presnall, D.C., Gudfinnsson, G.H., Walter, M.J., 2002. Generation of mid-ocean ridge basalts at pressures from 1 to 7 GPa. Geochimica et Cosmochimica Acta 66, 2073–2090.

Puziewicz, J., 2005. Litospheric mantle beneath SW Poland. In: Puziewicz, J. (Ed.), VI Meeting of the Mineralogical Society of Poland. Mineralogical Society of Poland, Krościenko, pp. 184–187.

Sawicki, L., 1995. Geological map of Lower Silesia with adjacent Czech and German territories (without Quarternary deposits). Polish Geological Institute.

Shaw, C.S.J., 1999. Dissolution of orthopyroxene in basanitic magma between 0.4 and 2 GPa: further implications for the origin of Si-rich alkaline glass inclusions in mantle xenoliths. Contributions to Mineralogy and Petrology 135, 114–132.

Šibrava, V., Havliček, P., 1980. Radiometric age of Plio–Pleistocene volcanic rocks of the Bohemian Massif. Véstník Ustředního Ústavu Geologického 55, 129–139.
Touron, S., Renac, C., O'Reilly, S.Y., Cottin, J.Y., Griffin, W.L., 2008. Characterization of the metasomatic agent in mantle xenoliths from Deves, Massif Central (France) using coupled in situ trace-element and O, Sr and Nd isotopic compositions. Geological Society, London, Special Publications 293, 177–196.
Turniak, K., Mazur, S., Wysoczański, R., 2000. SHRIMP zircon geochronology and geochemistry of the Orlica – Śnieżnik gneisses (Variscan belt of Central Europe) and their tectonic implications. Geodinamica Acta 13, 293–312.
Wells, P.R.A., 1977. Pyroxene thermometry in simple and complex systems. Contributions to Mineralogy and Petrology 62, 129–139.
Wierzchołowski, B., 1993. Stanowisko systematyczne i geneza sudeckich skał wulkanicznych. Archiwum Mineralogiczne 49, 199–235 (in Polish).
Wilson, M., Downes, H., 2006. Tertiary–Quaternary intra-plate magmatism in Europe and its relationship to mantle dynamics. Geological Society, London, "European Lithosphere Dynamics" Memoir, 147–166.
Zangana, N.A., Downes, H., Thirlwall, M.F., Hegner, E., 1997. Relationship between deformation, equilibration temperatures, REE and radiogenic isotopes in mantle xenoliths (Ray Pic, Massif Central, France): an example of plume-lithosphere interaction? Contributions to Mineralogy and Petrology 127, 187–203.
Zangana, N.A., Downes, H., Thirlwall, M.F., Marriner, G.F., Bea, F., 1999. Geochemical variation in peridotite xenoliths and their constituent clinopyroxenes from Ray Pic (French Massif Central): implications for the composition of the shallow lithospheric mantle. Chemical Geology 153, 11–35.